Laser Induced Breakdown Spectroscopy for In-Situ Monitoring of Laser Powder Bed Fusion Processing

Justin T. Krantz[1], Cody S. Lough[2], Ben Brown[2], Jinyu Yang[1], David B. Go[1,3], Robert G. Landers[1], Edward C. Kinzel[1]

[1]Department of Aerospace and Mechanical Engineering, University of Notre Dame, Notre Dame, IN 46556

[2]Kansas City National Security Campus, Kansas City, MO 64147

[3]Department of Chemical and Biomolecular Engineering, University of Notre Dame, Notre Dame, IN 46556

Abstract

A major challenge for laser powder bed fusion processes is identifying and addressing flaws in the as-built part. In-situ monitoring of the magnitude of radiation emitted from the vicinity of the melt pool largely corresponds to the temperature field. This has been correlated with the local porosity and microstructure of the part. However, the composition of the part can also vary, either because of processing conditions or differences in the powder. Spectroscopy has the potential to resolve material composition because spectral lines corresponding to atomic species present in the metal can be clearly observed. The line emission phenomena from ionization and excitation in the vapor plume is limited under standard LPBF conditions. Laser induced breakdown spectroscopy (LIBS) uses a pulsed laser to produce a localized plasma. This is demonstrated in LPBF using an ultrashort pulsed (USP) laser coaligned to the continuous wave (CW) process laser. The USP laser can be used to probe the melt pool and plume in-process, creating a plasma that is independent of the process conditions. This probing process has minimal adverse effects on the melt pool. LIBS can provide feedback about the local species content through time resolved spectroscopy and provides the potential for voxelwise composition information to be obtained from the material.

1. Introduction

Laser powder bed fusion (LBPF) is a metal powder based additive manufacturing (AM) process involving layerwise construction of three-dimensional parts. One downside of LBPF is that the part geometry and microstructure can have great variation with the processing conditions. Control of the processing conditions is crucial to creating high quality parts. Temperature distribution in LBPF has been widely studied with many techniques such as infrared monitoring, visual monitoring, and photodiodes [1-2]. Temperature distribution is crucial as the temperature history of a material determines the microstructure of the material. An additional challenge is the potential for local positional variation in elemental or phase composition [3]. Small variations in the species content of the material will change the microstructure, which will affect the phase composition and therefore performance of the material. In-situ monitoring has the potential to address these issues and allow for certification of the material properties in-process, which can

NSC-614-5638 09/2023
Unclassified Unlimited Release

increase reliability and reduce costs associated with the process. The integration of defect detection, process optimization, and real-time monitoring has the potential to increase LBPF-built part quality and consistency.

OES methods have previously been incorporated to monitor blown-powder techniques such as direct energy deposition (DED) [4-9]. Spectroscopic techniques in general have been more widely applied to DED and laser welding than LBPF, as DED and welding processes use a fixed heating zone in the machine frame, simplifying optical implantation since emission only needs to be read from the location of the fixed processing zone. A spectroscopic ratio is then used for process monitoring as it can be assumed that the absolute magnitude of spectral emission does not correspond to a change in composition. Dunbar *et al*. demonstrated the potential correlation between porosity of Inconel 718 manufactured by LPBF and the line-to-continuum ratios of chromium I (Cr I) emission at 520 nm [10]. Compared to blown-powder AM, implementation of OES as a process monitoring tool in PBF-based AM [10-11] can be challenging due to the movement of the melt pool during the process [12]. To address this, a coaxial OES system has been introduced with monitoring optics integrated into the laser path [12]. Parameters such as laser power, atmosphere, and pressure were found to vary OES signals, and the intensity of these signals was found to correlate with melt pool morphology [12]. This coaxial implementation illustrates the possibility of using OES for process feedback control.

A disadvantage to OES monitoring is that a high CW laser power is needed to achieve high line-continuum ratios from the melt pool alone, which can have a negative impact on part quality. Laser induced breakdown spectroscopy (LIBS) offers the ability to increase signal-to-noise ratio (SNR) of the emission signals as compared to conventional OES. Instead of directly sensing the emission induced by the process laser, the LIBS technique utilizes an additional powerful laser pulse to generate a highly localized plasma at the surface of the melt pool. This approach produces greater ionization and overall light emission, which leads to an enhancement in the SNR of spectra [13-15].

From an analysis of available literature, LIBS does not appear to have been applied to the LBPF process. However, it has been demonstrated with other AM methods. For example, the feasibility of incorporating a paraxial LIBS probe for in-situ quantitative multi-element analysis during the laser cladding process was demonstrated in [16]. While the LIBS data was less reproducible when sampling the hot solidified clad, meaningful results were still obtained in the characterization of the melt pool. Importantly, the properties of the fabricated feature remain unaffected, preserving the non-destructive nature of this technology [16]. The emission spectra of trace elements have relatively low intensity and are often overwhelmed by continuum background emission, especially at the initial phase of LIBS plasma expansion [17]. This phenomenon poses a challenge to achieving real-time chemical composition monitoring because intensified, gated recorders usually have a lower rate of data acquisition compared to the typical speed of an AM process. A different scheme of sampling at the metal powder feedstock jet mitigates the interference arising from melt pool radiation [18]. Whereas the reproducibility of the LIBS signal of this sampling scheme is relatively poor, it offers the potential of conducting online element analysis without the use of sophisticated spectrometers. LIBS signals of certain metallic emission spectra, such as Fe II at 495.16 nm, vary in the presence of manufacturing defects within the sampling target. As a result, spectral differences can serve as indicators of failures generated during the AM process [19], and machine learning algorithms were thereafter developed to facilitate the

recognition and categorization of various defects [20-21]. These investigations show the potential that this technique could be used with LBPF.

2. Experimental Setup

Experiments of LIBS were performed using a custom-built open LBPF system. The system consists of two coaligned lasers. One laser is an IPG Photonics YLR-500-AC continuous wave (CW) fiber laser with wavelength of 1070 nm. This laser is used to melt the powder and perform the laser powder bed fusion process at powers up to 500 W. The second laser is a Pharos PH1-20 ultrafast pulsed laser with wavelength of 1030 nm. This laser has a pulse width of 290 fs and can achieve up to 20 W of power at 200 kHz repetition frequency. This laser is used for precise micromachining which enables the option of performing LIBS studies.

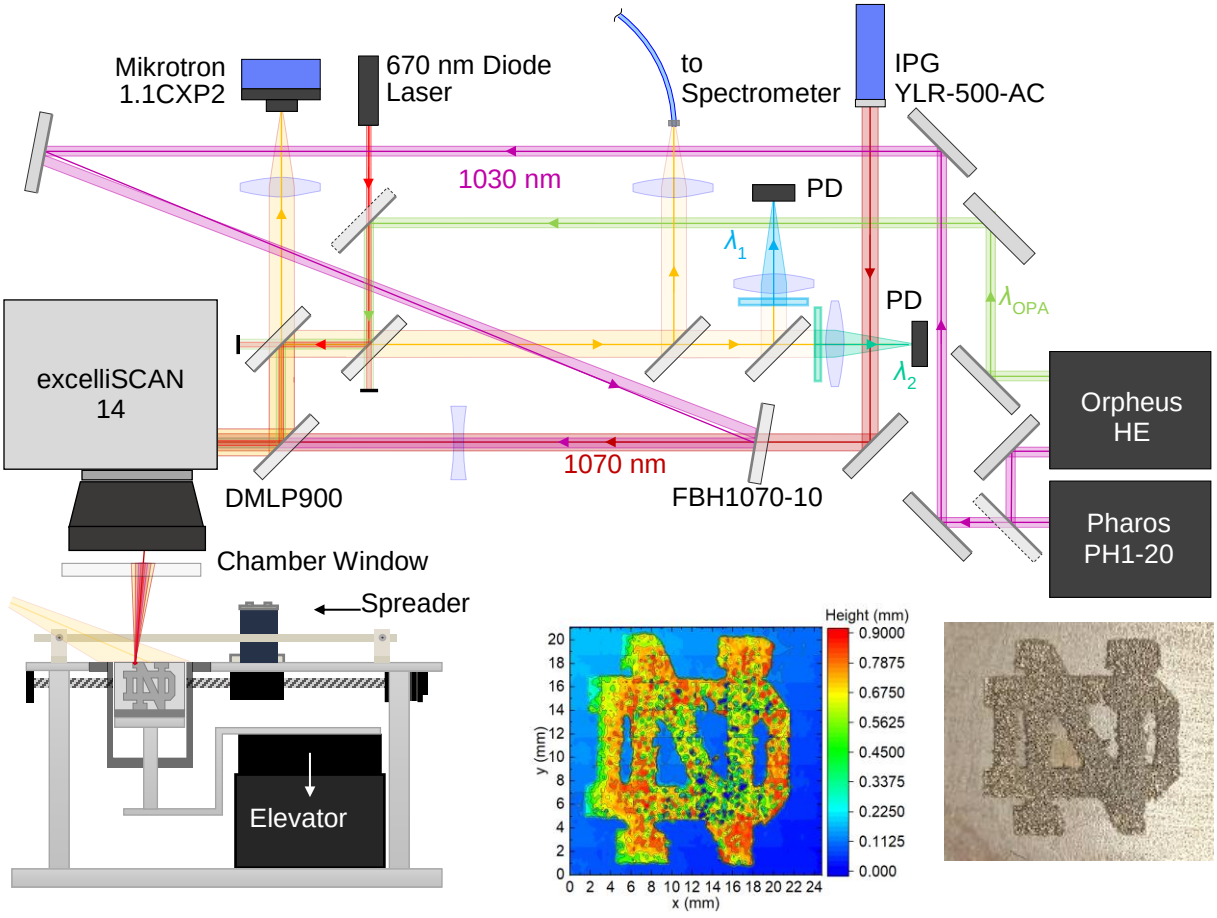

Figure 1: Illustration of optical components for open LBPF system. The inset show an as produced photograph and optical profilometer scan of an interlocking ND part.

The lasers positioning is controlled by a SCANLAB excelliSCAN14 galvo with the lasers focused through a f-theta lens with focal length of 163 mm. The laser beam diameters were measured to be 20 µm at the focal point. Emission spectra were collected using an Ocean Optics USB4000 spectrometer, which is coaligned to the lasers through the scanhead. A diagram of the

optical components of the system is illustrated in Fig. 1. This setup also provides atmospheric control. The chamber system allows for the ability to control pressure from 0.01 atm to 10 atm.

3. Results and Discussion

Experiments were performed to compare the signal quality of OES to LIBS during LBPF processing. All spectroscopy readings were taken under an argon atmosphere at near atmospheric pressure, with 304 stainless steel (SS304) chosen as the material of interest due to its ease of use and wide array of applications. All presented spectral signals were obtained with an exposure time of 100 ms. The first point of interest is the appearance of recorded OES signals. These signals were used as the baseline for comparison to LIBS signals. OES signals were recorded by only processing with the CW processing laser. These signals would be able to be collected with any typical LBPF setup. Figure 2a contains examples of typical OES signals collected from the process, and Figure 2b shows the variation of intensity of the Cr I emission line at a wavelength of 520.6 nm with the process laser power. This emission line is selected because it is the most prominent for SS304 over the visible range. Note that a strong blackbody radiation is observed in the OES signals in Figure 2a. This is one of the major challenges with applying OES to LBPF processes, as the large blackbody radiation from the plume can obscure the spectral signals from the material.

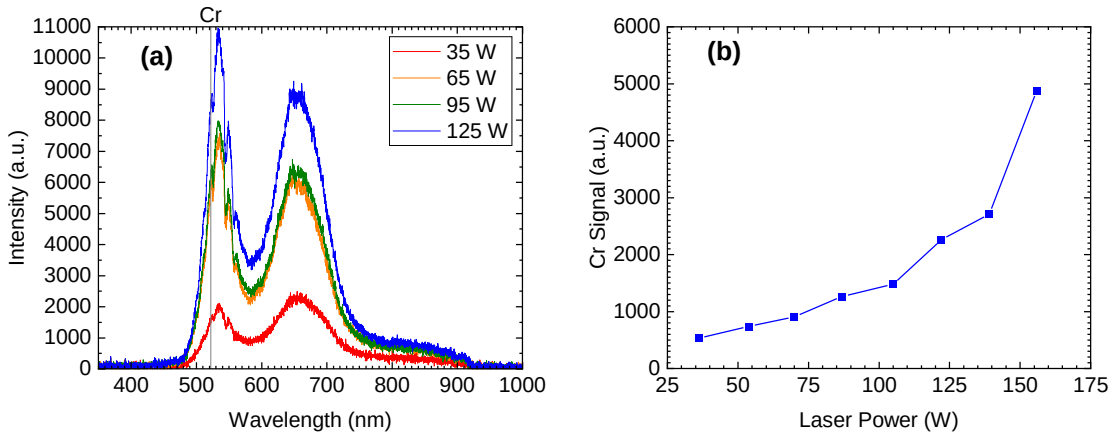

Figure 2: (a) Optical emission spectroscopy signals for four different process laser powers. (b) Chromium peak intensity at 520 nm as a function of processing laser power.

The OES results can be contrasted with the results from LIBS spectra. In this experiment, only the pulsed ultrafast laser was used to ablate a small amount of material to create a plasma. The emission from this plasma was then read by the spectrometer. All LIBS spectra presented in Fig. 3 were obtained using the same process parameters as the OES spectra in Fig. 2. It can be seen that the Cr signals at 520 nm are much stronger in terms of signal-noise ratio than the signals from the OES data. This is the case regardless of the input laser power from the ultrafast laser for the material. In all cases, the laser was run at 10 kHz repetition rate, with the laser pulse energy varied as shown in the graph.

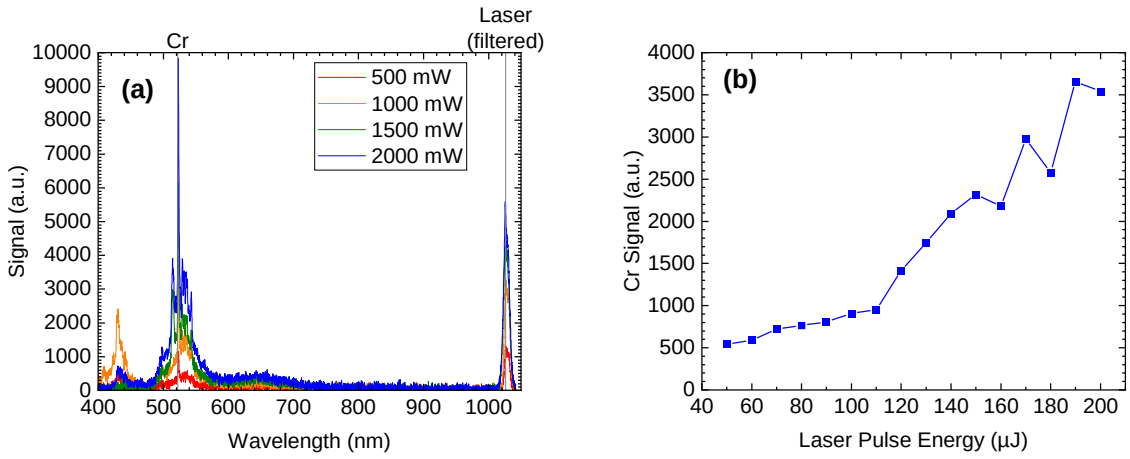

Figure 3: (a) Laser induced breakdown spectroscopy signals for four different ultrafast laser powers. (b) Chromium peak intensity at 520 nm as a function of ultrafast laser power.

LIBS spectral results from laser machining are not representative of the actual manufacturing conditions for LPBF. To create a realistic representation of the spectral sensing conditions, both lasers were active simultaneously. The ultrafast pulsed laser still excites the processing region to create a plume, but this occurs while the CW processing laser is on to create a part. Comparison of the spectral signals for having both lasers running to each laser individually demonstrates the increase in SNR from adding the ultrafast laser. An example comparison with the laser parameters of 10 kHz, 100 µJ pulse energy for the ultrafast laser and 175 W for the processing laser is in Fig. 4. In comparison to conventional OES, the spectral readings from having the ultrafast laser further excite the material retains the advantage of increasing SNR. This shows the potential of using LIBS for in-situ process monitoring in LBPF systems. Another interesting feature of the spectra obtained from firing both lasers simultaneously is that the blackbody radiation is decreased when compared to the scenario where only the process laser is firing. The cause of this change in the blackbody radiation will be an area of future study.

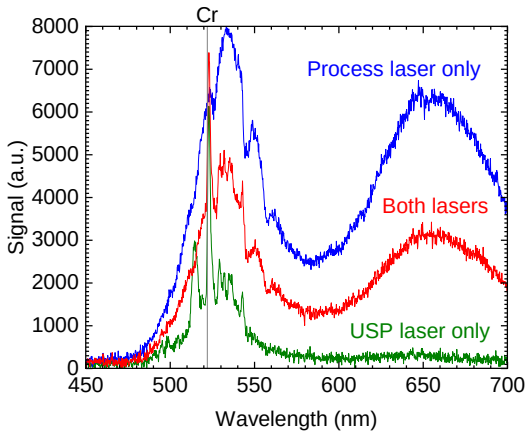

Figure 4: Comparison between spectral signals with one laser on at a time to spectral signals from both lasers on, with consistent laser parameters

The ability to monitor the spectral signal in-situ and in-process provides the potential for in-process readings of the chemical composition of the material. Tracking of the chemical composition is vital for LBPF processes due to the large effects that relatively small changes in chemical composition can have an appreciable influence on the phase composition and resulting mechanical properties of the material. Positional variation of chemical composition in a material can also negatively affect the properties of the material. Composition of LBPF structures can vary based on the dwell time of the melt pool. This can particularly cause issues at the edges of a part, where the dwell time differs from the bulk material. Figure 5 is a scanning electron microscope (SEM) image of a sample manufactured at 175 W laser power and 500 mm/s scan speed with skywriting scan strategy. This image reveals the change in morphology that can be observed at the edge of a sample.

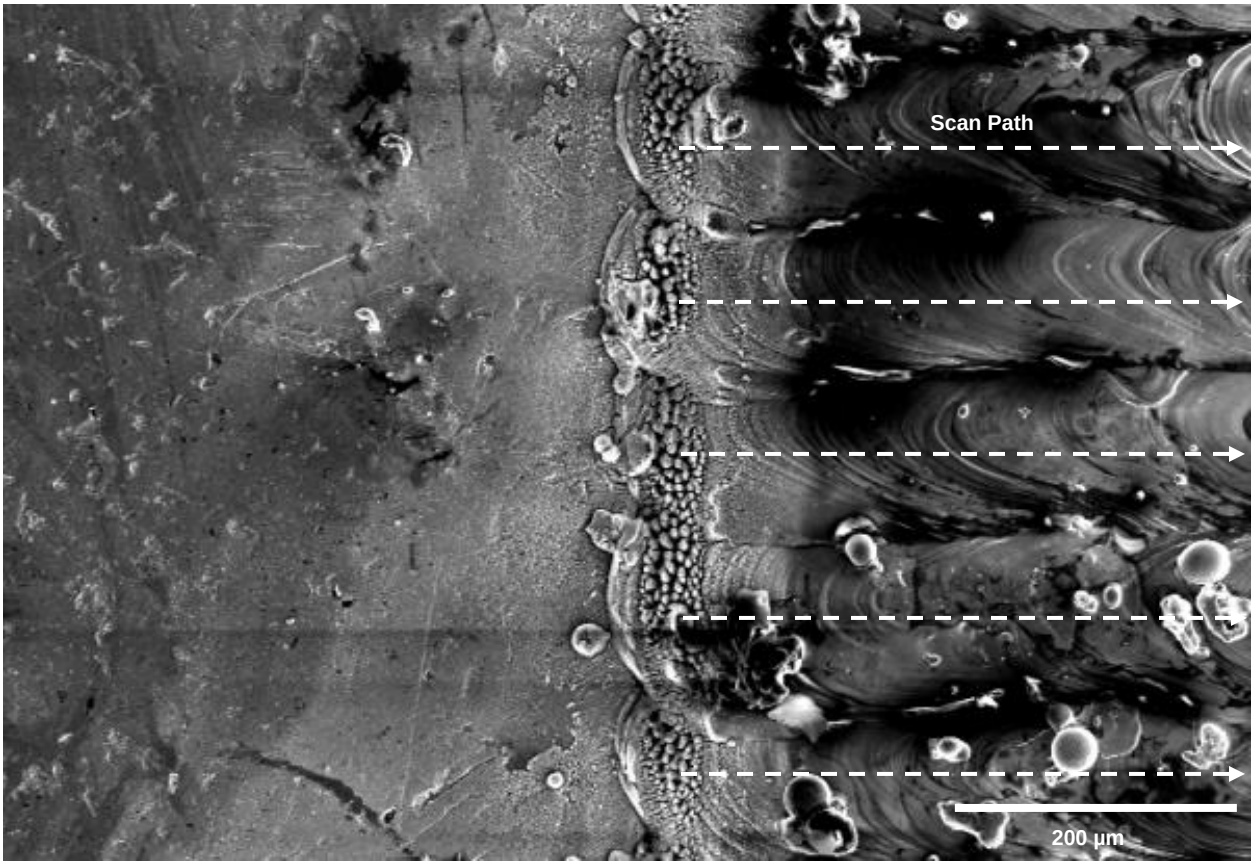

Figure 5: SEM image of an edge of a part

Chemical composition analysis also reveals changes in the material at the edge of the part. Electron dispersive x-ray spectroscopy (EDS) was also performed on samples to examine the variation in chemical composition with position. Figure 6 shows the EDS results taken at the edge of the sample, with chromium composition found to be depleted in a manner that matches the morphological change observed in the material.

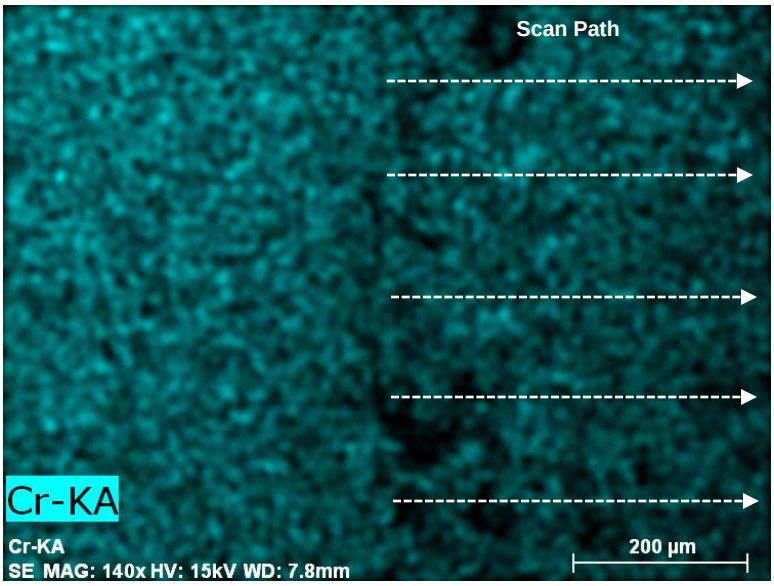

Figure 6: EDS mapping for Cr composition at the edge of a part

EDS results were also collected at this position in the sample for other elements. Iron and manganese were chosen as elements of interest for the EDS results as both elements are present in stainless steel samples. In comparison to the EDS mapping for chromium, iron and manganese both do not experience the same amount of depletion at the edges of the sample. Having the ability to map this composition in real time will allow for the potential to adapt to compositional differences in the material.

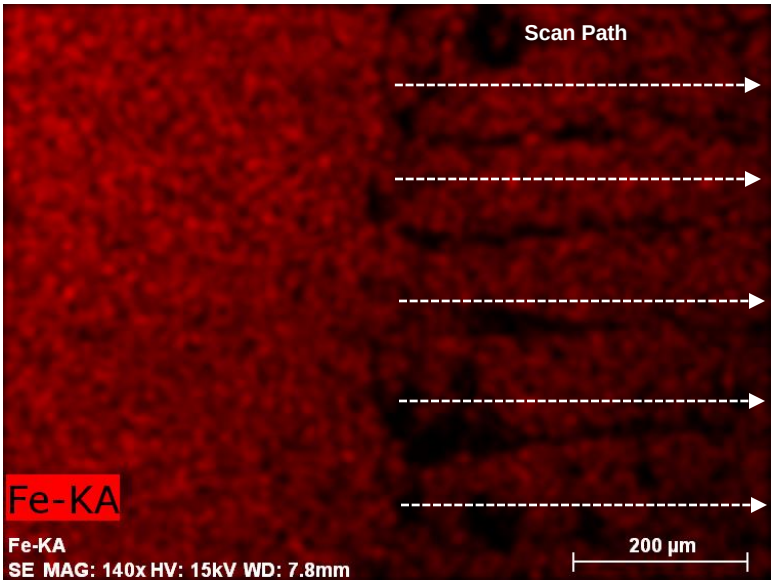

Figure 7: EDS mapping for Fe composition at the edge of a sample

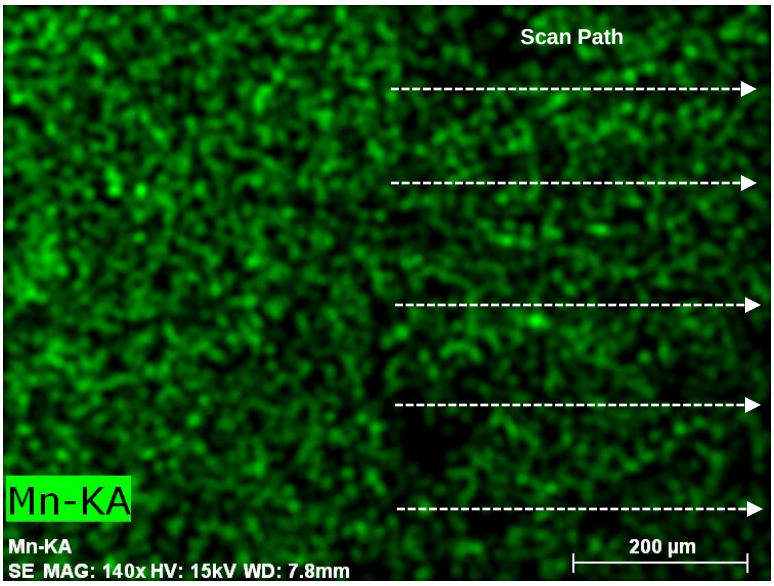

Figure 8: EDS mapping for Mn composition at the edge of a sample

Chromium content in the bulk material is also affected by the laser parameters used for creating LBPF parts. Identification of the chromium content in-process allows for the potential for feedback control to dynamically adjust laser parameters in process. Scan speed is one such parameter. Several samples were fabricated with the LBPF system at 175 W laser input power from the CW laser. Scan speed was varied from 5 mm s^{-1} up to 300 mm s^{-1} , with particularly low scan speeds intentionally included in an attempt to elicit a large change in the chromium content of the material. The chromium content of each sample was then measured via EDS. The chromium content and chromium/iron ratio in the material are both compared in Figure 9. Chromium content was found to have a strong dependence on laser scan speed, with it being particularly low at very low scan speeds.

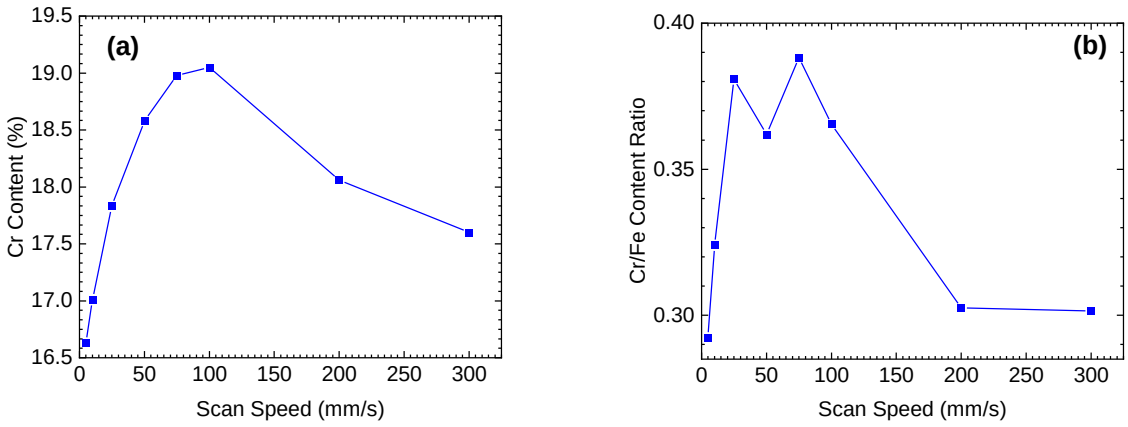

Figure 9: (a) EDS results for Cr content in the sample with varying scan speed (b) EDS results for Cr/Fe content ratio in the sample with varying scan speed

The ability to resolve elemental composition via LIBS allows for the potential to create a voxelwise representation of the composition of the material. This could then be correlated to features in the part to serve as process monitoring. A goal of this project in the future is to be able to increase the collection speed of spectral data thanks to the increased signal quality from LIBS to be able to create a high resolution layerwise composition map of the material.

4. Summary and Conclusions

This paper demonstrated the application of LIBS to LBPF processing. LIBS was demonstrated to have a marked increase on the signal-noise ratio of chromium emission peaks in comparison to conventional OES. Chromium content for stainless steel LBPF was observed to vary with both the laser power and position in the build. This variation in composition can affect the resulting properties of the material. The increased signal-noise ratio achievable by LIBS provides the potential ability to create a voxelized mapping of the composition of the material in-process. In-process monitoring provides the potential to quickly quantify part quality with the ability to detect defect formation. Future work for this project will involve increasing the frequency of spectral collection to allow for the creation of a three-dimensional map of composition in the material, with the opportunity to use the ultrafast laser to repair any identified defects in-situ. Plasma dynamics will vary the LIBS signal, as a denser plume will result in a brighter plasma. Plume density is dependent on pressure, and the effects of pressure on LIBS signal quality will be studied. LIBS monitoring will also be extended to other materials commonly produced via LBPF such as aluminum and titanium, as both metals have strong peaks in the visible detection range of this setup.

5. Acknowledgement

This work was funded by the Department of Energy's Kansas City National Security Campus, operated by Honeywell Federal Manufacturing & Technologies, LLC, under contract number DE-NA0002839.

6. References

[1] T. Liu, C.S. Lough, H. Sehhat, Y.M. Ren, P.D. Christofides, E.C. Kinzel, M.C. Leu, In-situ infrared thermographic inspection for local powder layer thickness measurement in laser powder bed fusion, Additive Manufacturing. 55 (2022) 102873. https://doi.org/10.1016/j.addma.2022.102873.

[2] L. Scime, J. Beuth, Anomaly detection and classification in a laser powder bed additive manufacturing process using a trained computer vision algorithm, Additive Manufacturing. 19 (2018) 114–126. https://doi.org/10.1016/j.addma.2017.11.009.

[3] N. Takata, M. Liu, H. Li, A. Suzuki, M. Kobashi, Fast scanning calorimetry study of Al alloy powder for understanding microstructural development in laser powder bed fusion, Materials & Design. 219 (2022) 110830. https://doi.org/10.1016/j.matdes.2022.110830.

[4] L. Song, J. Mazumder, Real Time Cr Measurement Using Optical Emission Spectroscopy During Direct Metal Deposition Process, IEEE Sensors Journal. 12 (2012) 958–964. https://doi.org/10.1109/JSEN.2011.2162316.

[5] A.R. Nassar, T.J. Spurgeon, E.W. Reutzel, Sensing Defects during Directed-Energy Additive Manufacturing of Metal Parts using Optical Emissions Spectroscopy, in: University of Texas at Austin, 2014. https://doi.org/10.26153/tsw/15684.
[6] L. Song, W. Huang, X. Han, J. Mazumder, Real-Time Composition Monitoring Using Support Vector Regression of Laser-Induced Plasma for Laser Additive Manufacturing, IEEE Transactions on Industrial Electronics. 64 (2017) 633–642. https://doi.org/10.1109/TIE.2016.2608318.
[7] C.B. Stutzman, A.R. Nassar, E.W. Reutzel, Multi-sensor investigations of optical emissions and their relations to directed energy deposition processes and quality, Additive Manufacturing. 21 (2018) 333–339. https://doi.org/10.1016/j.addma.2018.03.017.
[8] J. Shin, J. Mazumder, Composition monitoring using plasma diagnostics during direct metal deposition (DMD) process, Optics & Laser Technology. 106 (2018) 40–46. https://doi.org/10.1016/j.optlastec.2018.03.020.
[9] W. Ren, Z. Zhang, Y. Lu, G. Wen, J. Mazumder, In-Situ Monitoring of Laser Additive Manufacturing for Al7075 Alloy Using Emission Spectroscopy and Plume Imaging, IEEE Access. 9 (2021) 61671–61679. https://doi.org/10.1109/ACCESS.2021.3074703.
[10] A.J. Dunbar, A.R. Nassar, Assessment of optical emission analysis for in-process monitoring of powder bed fusion additive manufacturing, Virtual and Physical Prototyping. 13 (2018) 14–19. https://doi.org/10.1080/17452759.2017.1392683.
[11] M. Montazeri, A.R. Nassar, A.J. Dunbar, P. Rao, In-process monitoring of porosity in additive manufacturing using optical emission spectroscopy, IISE Transactions. 52 (2020) 500–515. https://doi.org/10.1080/24725854.2019.1659525.
[12] C.S. Lough, L.I. Escano, M. Qu, C.C. Smith, R.G. Landers, D.A. Bristow, L. Chen, E.C. Kinzel, In-situ optical emission spectroscopy of selective laser melting, Journal of Manufacturing Processes. 53 (2020) 336–341. https://doi.org/10.1016/j.jmapro.2020.02.016.
[13] D.W. Hahn, N. Omenetto, Laser-Induced Breakdown Spectroscopy (LIBS), Part I: Review of Basic Diagnostics and Plasma–Particle Interactions: Still-Challenging Issues Within the Analytical Plasma Community, Appl. Spectrosc., AS. 64 (2010) 335A-366A.
[14] D.W. Hahn, N. Omenetto, Laser-Induced Breakdown Spectroscopy (LIBS), Part II: Review of Instrumental and Methodological Approaches to Material Analysis and Applications to Different Fields, Appl Spectrosc. 66 (2012) 347–419. https://doi.org/10.1366/11-06574.
[15] A. Bengtson, Laser Induced Breakdown Spectroscopy compared with conventional plasma optical emission techniques for the analysis of metals – A review of applications and analytical performance, Spectrochimica Acta Part B: Atomic Spectroscopy. 134 (2017) 123–132. https://doi.org/10.1016/j.sab.2017.05.006.
[16] V.N. Lednev, P.A. Sdvizhenskii, R.D. Asyutin, R.S. Tretyakov, M.Ya. Grishin, A.Ya. Stavertiy, S.M. Pershin, In situ multi-elemental analysis by laser induced breakdown spectroscopy in additive manufacturing, Additive Manufacturing. 25 (2019) 64–70. https://doi.org/10.1016/j.addma.2018.10.043.
[17] B. Lei, B. Xu, J. Wang, J. Li, Y. Wang, J. Tang, W. Zhao, Y. Duan, Time-resolved characteristics of laser induced breakdown spectroscopy on non-flat samples by single beam splitting, RSC Advances. 10 (2020) 39553–39561. https://doi.org/10.1039/D0RA06582J.
[18] P. A. Sdvizhenskii, V. N. Lednev, R. D. Asyutin, M. Ya. Grishin, R. S. Tretyakov, S. M. Pershin, Online laser-induced breakdown spectroscopy for metal-particle powder flow analysis during additive manufacturing, Journal of Analytical Atomic Spectrometry. 35 (2020) 246–253. https://doi.org/10.1039/C9JA00343F.

[19] V.N. Lednev, P.A. Sdvizhenskii, R.D. Asyutin, R.S. Tretyakov, M.Y. Grishin, A.Y. Stavertiy, A.N. Fedorov, S.M. Pershin, In situ elemental analysis and failures detection during additive manufacturing process utilizing laser induced breakdown spectroscopy, Opt. Express, OE. 27 (2019) 4612–4628. https://doi.org/10.1364/OE.27.004612.
[20] J. Lin, J. Yang, Y. Huang, X. Lin, Defect identification of metal additive manufacturing parts based on laser-induced breakdown spectroscopy and machine learning, Appl. Phys. B. 127 (2021) 173. https://doi.org/10.1007/s00340-021-07725-3.
[21] J. Lin, J. Yang, Y. Huang, X. Lin, C. Che, Laser-induced breakdown spectroscopy and stoichiometry to identify various types of defects in metal-additive manufacturing parts, Journal of Analytical Atomic Spectrometry. 38 (2023) 1501–1511. https://doi.org/10.1039/D3JA00060E.